SUPPLEMENTARY INFORMATION for:

"The outcome of TGF-β antagonism in metastatic breast cancer models *in vivo* reflects a complex balance between tumor-suppressive and pro-progression activities of TGF-β"
by Yang *et al*. CCR-19-2370-R

INDEX:

Supplementary Tables are in a separate Excel file with 4 tabs:

Supplementary Table S1: Cell line sources, characteristics, culture conditions and metastasis assay formats
Supplementary Table S2: InhibMet and StimMet gene signatures
Supplementary Table S3: Antibodies used for Western blots and SimpleWestern capillary nano-immunoassays
Supplementary Table S4: Immunostaining reagents and conditions for immunohistochemical characterization of the tumor panel

SUPPLEMENTARY MATERIALS AND METHODS

Ethics statement

All animal studies were conducted under protocol LC-070 approved by the Animal Care and Use Committee of the National Cancer Institute. The Frederick National Laboratory and the Center for Cancer Research are accredited by AALAC International and follow the Public Health Service Policy for the Care and Use of Laboratory Animals. Animal care was provided in accordance with the procedures outline in the "Guide for Care and Use of Laboratory Animals" (National Research Council; 2011, National Academies Press; Washington, DC).

Model acquisition and cell culture

Metastatic murine mammary cancer cell lines were obtained from the originating laboratories and/or investigators as detailed in Supplementary Table S1. Cell lines were maintained in culture using growth media and optimal split ratios as indicated in Supplementary Table S1. Care was taken not to use very high split ratios and not to let the cells go confluent at any time. All lines were tested and shown to be free of mouse viral pathogens, and were tested for

mycoplasma using the LookOut Mycoplasma PCR Detection Kit (Sigma Cat# MP0035-1KT). Cells were injected into mice within 2-3 passages from thawing. Genomic, transcriptomic and some immunohistochemical characterization of these allograft models has been previously described (1).

Therapeutic antibodies. A mouse monoclonal antibody 1D11 (IgG1κ) that neutralizes all three isoforms of TGF-β was obtained from Genzyme Corp., Framingham, MA, or purchased from BioXCell (InVivoPlus Catalog #BP0057). The isotype-matched IgG antibodies 13C4 (Genzyme Corp) or MOPC21 (BioXCell InVivoPlus Catalog #BP0083) were used as the treatment control.

Animal studies, antibody treatment and tissue collection

We aimed to find conditions that gave lung metastases in at least 60% of the mice on study, and with metastatic burden being readily detectable within 60 days of tumor cell implantation. The preferred assay format was orthotopic implantation of the primary tumors, with surgical resection when tumors reached 0.5-0.8cm diameter. The #4 mammary fatpad (mfp) was surgically exposed for implantation to ensure that cells were actually implanted into the mfp rather than just in the vicinity. If metastatic efficiency was too low from the #4 mfp, the #2 mfp was used. For the EMT6 model, cells were implanted in a 1:1 mix with reduced growth factor Matrigel (BD Biosciences). If metastatic frequency following tumor resection was low, the model was run without resection (E0771, MVT1, R3T). If metastatic frequency was still undesirably low following orthotopic implantation, cells were introduced into the mice via the tail vein (MET1, F3II, TSAE1). The detailed experimental conditions used to generate metastases from all these models in our facility are given in Supplementary Table S1. Tumor cells were implanted or injected into strain-matched virgin female mice aged 6-8 weeks. After tumor cell implantation, mice were randomly assigned by cage (n-5 mice) between treatment groups. Antibodies were dosed at 5mg/kg bodyweight intraperitoneally, three times a week for the duration of the experiment. For most experiments, antibody treatment was initiated at day +1 after tumor cell implantation. However, where indicated in the text, antibody treatment was delayed until primary tumors were well-established (>3mm diam), or immediately before or after primary tumor resection. Technicians were blinded to identity of treatment groups. At the experimental endpoint, mice were euthanized by carbon dioxide narcosis followed by

thoracotomy. Primary tumors at resection or endpoint (in no resection models) were weighed, bisected and snap frozen in liquid nitrogen for molecular analyses or fixed in 10% neutral buffered formalin (NBF). Lungs were inflated with 10% NBF, and fixed for paraffin embedding and histological analysis. Lung metastatic burden was assessed by blinded counting of histologically-evident metastatic lesions on hematoxylin-eosin (H&E) stained sections of individual lung lobes. To account for any effect of therapy on the primary tumor affecting the metastatic burden, the number of lung metastases was normalized to the primary tumor weight at resection to generate a "metastatic index". There is a weak trend towards an overall higher metastatic burden in the control groups for models where an inhibitory effect of the therapeutic antibodies was seen (InhibMet models) compared with the other groups. This is because, based on small-scale pilot studies, we selected cell innocula for the definitive studies that would best allow us to see a significant decrease (InhibMet models; higher metastatic burden in control state) or increase (StimMet models; lower metastatic burden in control state) in metastasis in response to therapy.

Quantitation of TGF-β1,2 and 3 in tumors and plasma

For accurate quantitation of total TGF-β levels in primary tumors from the different models, acid-ethanol extraction of frozen tissues was performed as described in detail elsewhere (2). Blood was collected by retro-orbital puncture and platelet-poor plasma was prepared as previously described, taking care to minimize platelet contamination and degranulation at all steps (3). TGF-β isoforms were quantitated using the TGF-β Premixed Luminex Performance Assay kits from R&D Systems (#FCSTM17) with detection using a Bio-Plex MAGPIX reader. Acid-ethanol extracts of tumors or normal mammary gland were generally diluted 1:5 with RD5-49 buffer (supplied with the kit) while plasma samples were activated with HCl, neutralized and diluted in RD6-50 buffer according to the manufacturer's instructions. TGF-β levels in tumors were normalized to the weight of the tissue sample extracted and are expressed as ng TGF-β/g tissue. Reported TGF-β levels derived from measurements on acid-ethanol extracts are corrected for the 50% sample loss we have observed in processing the acid-ethanol extracts which was determined by addition of trace ^{125}I-labeled TGF-β1 to parallel samples prior to extraction (4).

Conventional Western blots and SimpleWestern quantitative nanocapillary immunoassays. TGF-β signaling in tumor cells in culture was assessed by culturing cells in serum-free medium overnight, followed by addition of 2ng/ml TGF-β or vehicle. At t=0, 2 and 24-hours**,** cells were lysed in RIPA buffer (ThermoScientific #89900)and run on 10% gels (BioRad #456-1036) for Western blotting with antibodies listed in Suppl. Table S3. For TGF-β signaling in control or antibody treated primary tumors, snap frozen tumor samples (4-5 tumors/model) were lysed in T-PER buffer (Thermo Scientific) with HALT inhibitors, for target quantification by an automated capillary electrophoresis nano-immunoassay system (Peggy Sue Simple Western™, ProteinSimple, San Jose, CA). The tumor protein lysate (40-60 ng/target) was analyzed according to the manufacturer's instructions using the antibodies listed in Suppl. Table S3.

Immunohistochemistry and brightfield proximity ligation assay

Immunohistochemistry. Three representative primary tumors for each model were immunostained for Ki67 (proliferation), Caspase3 (apoptosis), CD34 (angiogenesis), CD45 (pan-leukocyte), CD3 (T-cell), CD4 (T-cell subset), CD8 (T-cell subset), Ly6G (granulocyte), F4/80 (macrophage) markers. Details of the antibodies and conditions used for immunostaining are given in Suppl. Table S4. All immunostaining steps from deparaffinization through counterstaining were performed using a BondMax Autostainer (Leica Biosystems). Immunostained slides were scanned with a 20x objective using an Aperio Scanner. Images of the entire tumor section were manually segmented to exclude regions of intra-tumoral necrosis and of stroma surrounding the tumor, and automated Aperio-designed algorithms were run to assess the positive cells as % total nuclei in the segmented region (Ki67, caspase3 and leukocyte markers) or microvessel density (CD34: # microvessels/μm^2). For F4/80, only nuclei that scored 3+ were counted as some of the tumor models showed low level staining for F4/80 in the tumor cells. ***Proximity ligation assay.*** Brightfield proximity ligation assays for canonical TGF-β SMAD complexes (SMAD2/3 with SMAD4), canonical BMP SMAD complexes (SMAD1/5/9 with SMAD4) or "mixed SMAD" complexes (SMAD2/3 with SMAD1/5/9) were performed on FFPE-embedded tissue using custom antibodies as previously described (5). Three primary tumors for each model were stained. The PLA signal was scored blinded on a scale of 0-3 by two independent observers and discrepant scores were resolved by consensus.

Genetic inhibition of TGF-β signaling in tumor cells. Stable knockdown of SMAD2 and SMAD3 in MVT1 cells was done by lentiviral transduction with shRNA against SMAD2 (5'CGCACTTGCTCTGAAATTTGCCTC (#7114-X02), SMAD3 (5'-GGCCATCACCACGCAGAAC-3')(#7114-X03), or GFP (5'-AAGACCCGCGCCGAGGTGAAG-3')(#7114-X01) cloned into the pLKO.1-TRC lentiviral vector, followed by puromycin selection. Knockdown was validated by Western blot analysis. A dominant negative type II TGF-β receptor (*dnTgfbr2*) consisting of the first 245 amino acids of the mouse *Tgfbr2* gene with 3 copies of a FLAG tag added to the C-terminus was cloned by Gateway multisite cloning into a lentiviral backbone with a neomycin selection cassette and a chick γ-actin promoter (CAG) to drive dnTGFBR2 expression (#13696-M07-676). An identical construct lacking the *dnTgfbr2* insert was used as a control (#13696-M08-686). Cells were transduced and selected for two weeks with neomycin before injection into mice.

In vitro assays.

Proliferation. Cell proliferation was assessed by tritiated thymidine incorporation essentially as described (6). Briefly, cells were seeded in complete medium and switched to serum-free medium for 18 hours prior to addition of 5ng/ml TGF-β for 22 h. After a 2 hour pulse with ^{3}H-thymidine (PerkinElmer #NET027Z001 MC), cultures were washed and ^{3}H-Thy incorporation was assessed using a Beckman scintillation counter. ***Apoptosis***. Cells were seeded in complete medium and then switched to medium containing 0.2% serum, and treated with 5ng/ml TGF-β or vehicle for 24 hours. Apoptosis was assessed using the Cell Death Detection ELISA Plus (Roche) according to manufacturer's instructions. ***Migration and invasion.*** Cells were seeded at 5000-50,000 cells/well into the upper chamber of 24-well migration (BD Falcon HTS 24 Multiwell Insert System) or invasion (BD BioCoat 8μm pores size Cat # 354480) plates. After allowing cells to attach for 3-4 hours, cells were switched to low serum medium in the upper chamber, and TGF-β (5ng/ml) or vehicle were added to upper and lower chambers. After 24-48 hours, cells on the lower side of the insert were fixed, visualized with 0.05% Crystal Violet and counted under the microscope. ***Clonogenicity.*** Cells were seeded at 150-300 cells/well in 6-well plates in low-serum medium (2% FBS) with 5 ng/ml TGF-β or vehicle. After culturing for 10 days, cells were fixed in methanol, stained with crystal violet, imaged using a ChemiDoc Touch Imaging System (Bio-Rad), and colonies > 50 cells were counted using the MultiImage II

software (Alpha Innotech). ***Tumorsphere formation.*** Cells were cultured for 3-8 days in low serum medium (2% FBS) with 2ng/ml TGF-β or vehicle**.** Cells were then trypsinized and seeded at 10,000 cells/well in a 9:4 mix of Methocult H4100 (Stemcell Technologies Cat# 04100) and MammoCult (StemCell Technologies Cat #05620) in 24-well ultralow attachment plates (Corning #3473). After culturing for 7-13 days, tumorspheres were imaged, sized and quantitated using a Celigo Imaging Cytometer (Nexcelcom).

Genomic characterization of tumor cell lines

Copy number variant (CNV) analysis. RNA-free genomic DNA (gDNA) from the 12 cell lines was analyzed using the Affymetrix® Mouse Diversity Genotyping array, as previously described (1). Data from normal tissue of matched mouse strains (http://cgd.jax.org/datasets/diversityarray/CELfiles.shtml) were used as references to identify strain-specific regions of copy number gain or loss, which were then removed from the processed datasets. CNV data have been deposited in GEO under accession # GSE69902.

Single nucleotide variant (SNV) analysis. Exome libraries were prepared from cell line gDNA and deep sequencing and variant calling were performed after filtering out mouse strain-specific single nucleotide polymorphisms (SNPs) as previously described (1). Mean target coverage depth was 85-141X with 84% of regions having >30x coverage. Exonic SNPs were identified and variants were classified as synonymous or non-synonymous by ANNOVAR. Variants that were present in all cell lines from the same strain background, and variants with a Phred-scaled quality score of <30 were removed. SNV data have been deposited in GEO under accession # GSE69902. ***Neoantigen load.*** High quality non-recurrent, non-synonymous variants were then analyzed for their potential to function as neoantigens. 25-amino acid peptides with a mutation at position 13 were used for MHC class I binding analysis using the NetMHC algorithm (http://www.cbs.dtu.dk/services/NetMHC/26515819.pdf).

Gene expression analysis

Primary tumors from cells implanted orthotopically into the #4 mammary fatpad of syngeneic mouse hosts were harvested when they reached 0.5-1.0 cm diameter. RNA was prepared from four representative tumors of each of the 12 models and hybridized to the Affymetrix Mouse Gene 1.0 ST array as previously described (1). After RMA normalization, unsupervised

hierarchical clustering and differential gene expression analysis were performed. The Kruskal-Wallis test identified 622 genes that were differentially expressed genes across the three therapeutic response classes (InhibMet, NoEff, StimMet) at an FDR of 0.005. For pairwise contrasts between individual response classes, t-tests with an FDR cutoff of 0.1 and an absolute fold difference of >=1.5 were used. Some data visualization (PCA and heatmaps) was done using Partek Genomics Suite 7.0. Differentially expressed genesets were analysed for enrichment of Hallmark genesets by using GSEA software (http://www.broad.mit.edu/gsea/) (7). The assignment of mouse models to the different intrinsic transcriptomic subtypes of human breast cancer, and the analysis of claudin-low status were as described previously (1). All mouse tumor array data have been deposited in GEO under accession number GSE96006.

De novo gene signature generation. To generate gene expression signatures that discriminated the StimMet and InhibMet response classes, the gene expression profiles of each class were compared individually against the remaining two classes. The top most significant differentially expressed genes (FDR≤0.01) for each contrast were selected and weighted by log2 fold expression difference to generate a StimMet and and InhibMet signature (Suppl Table S2). The relative score for these two signatures in different subtypes and histologic grades of human breast cancer was assessed in the METABRIC transcriptomic dataset of 2000 breast cancers (8).

Published gene signatures. A number of previously published gene signatures were tested for their ability to discriminate the three different therapeutic response classes. A TGF-β response signature (TBRS), comprising genes that reflect both tumor suppressive and tumor promoting activities of TGF-β was from Padua et al (9). The TGF-β/Smad3 tumor suppressor signature (TSTSS) which specifically isolates the tumor cell-autonomous tumor suppressive activities of TGF-β was from Sato et al. (10). A "TGF-β switch" signature was generated from seven genes whose expression had previously been suggested to determine whether TGF-β functions predominantly as tumor suppressor or tumor promoter (11-17). This signature was tested as the unweighted sum of the expression of the seven genes, or in a version where gene expression was weighted +1 (*Pspc1, Klf5, Ywhaz, Six1, Peak1*) or -1 (*Rassf1, Dab1*) based on the predicted direction of expression that favors the tumor promoting state. The cytotoxic T-cell signature was defined as the sum of the expression of *Cd8a, Cd8b1, Gzma, Gzmb* and *Prf1* (18). The IFNγ signature geneset used was the 18 gene interferon-γ based expanded immune gene signature from Ayers et al. (19).

SUPPLEMENTARY REFERENCES

1. Yang Y, Yang HH, Hu Y, Watson PH, Liu H, Geiger TR*, et al.* Immunocompetent mouse allograft models for development of therapies to target breast cancer metastasis. Oncotarget **2017** doi 10.18632/oncotarget.15695.
2. Flanders KC, Yang YA, Herrmann M, Chen J, Mendoza N, Mirza AM*, et al.* Quantitation of TGF-β proteins in mouse tissues shows reciprocal changes in TGF-β1 and TGF-β3 in normal vs neoplastic mammary epithelium. Oncotarget **2016** doi 10.18632/oncotarget.9416.
3. Kopp JB, Factor VM, Mozes M, Nagy P, Sanderson N, Bottinger EP*, et al.* Transgenic mice with increased plasma levels of TGF-β 1 develop progressive renal disease. Lab Invest **1996**;74(6):991-1003.
4. Danielpour D, Kim KY, Dart LL, Watanabe S, Roberts AB, Sporn MB. Sandwich enzyme-linked immunosorbent assays (SELISAs) quantitate and distinguish two forms of transforming growth factor-β (TGF-β 1 and TGF-β 2) in complex biological fluids. Growth Factors **1989**;2(1):61-71.
5. Flanders KC, Heger CD, Conway C, Tang B, Sato M, Dengler SL*, et al.* Brightfield proximity ligation assay reveals both canonical and mixed transforming growth factor-β/bone morphogenetic protein Smad signaling complexes in tissue sections. J Histochem Cytochem **2014**;62(12):846-63 doi 10.1369/0022155414550163.
6. Danielpour D, Dart LL, Flanders KC, Roberts AB, Sporn MB. Immunodetection and quantitation of the two forms of transforming growth factor-β (TGF-β 1 and TGF-β 2) secreted by cells in culture. J Cell Physiol **1989**;138(1):79-86 doi 10.1002/jcp.1041380112.
7. Subramanian A, Tamayo P, Mootha VK, Mukherjee S, Ebert BL, Gillette MA*, et al.* Gene set enrichment analysis: a knowledge-based approach for interpreting genome-wide expression profiles. Proc Natl Acad Sci U S A **2005**;102(43):15545-50 doi 10.1073/pnas.0506580102.
8. Curtis C, Shah SP, Chin SF, Turashvili G, Rueda OM, Dunning MJ*, et al.* The genomic and transcriptomic architecture of 2,000 breast tumours reveals novel subgroups. Nature **2012**;486(7403):346-52 doi nature10983 [pii];10.1038/nature10983 [doi].
9. Padua D, Zhang XH, Wang Q, Nadal C, Gerald WL, Gomis RR*, et al.* TGFβ primes breast tumors for lung metastasis seeding through angiopoietin-like 4. Cell **2008**;133(1):66-77.
10. Sato M, Kadota M, Tang B, Yang HH, Yang YA, Shan M*, et al.* An integrated genomic approach identifies persistent tumor suppressive effects of transforming growth factor-β in human breast cancer. Breast Cancer Res **2014**;16(3):R57 doi bcr3668 [pii];10.1186/bcr3668 [doi].
11. Yeh HW, Hsu EC, Lee SS, Lang YD, Lin YC, Chang CY*, et al.* PSPC1 mediates TGF-β1 autocrine signalling and Smad2/3 target switching to promote EMT, stemness and metastasis. Nat Cell Biol **2018**;20(4):479-91 doi 10.1038/s41556-018-0062-y.
12. David CJ, Huang YH, Chen M, Su J, Zou Y, Bardeesy N*, et al.* TGF-β Tumor Suppression through a Lethal EMT. Cell **2016**;164(5):1015-30 doi 10.1016/j.cell.2016.01.009.

13. Xu J, Acharya S, Sahin O, Zhang Q, Saito Y, Yao J*, et al.* 14-3-3zeta turns TGF-β's function from tumor suppressor to metastasis promoter in breast cancer by contextual changes of Smad partners from p53 to Gli2. Cancer Cell **2015**;27(2):177-92 doi 10.1016/j.ccell.2014.11.025.
14. Micalizzi DS, Wang CA, Farabaugh SM, Schiemann WP, Ford HL. Homeoprotein Six1 increases TGF-β type I receptor and converts TGF-β signaling from suppressive to supportive for tumor growth. Cancer Res **2010**;70(24):10371-80.
15. Agajanian M, Campeau A, Hoover M, Hou A, Brambilla D, Kim SL*, et al.* PEAK1 Acts as a Molecular Switch to Regulate Context-Dependent TGFβ Responses in Breast Cancer. PLoS One **2015**;10(8):e0135748 doi 10.1371/journal.pone.0135748.
16. Pefani DE, Pankova D, Abraham AG, Grawenda AM, Vlahov N, Scrace S*, et al.* TGF-β Targets the Hippo Pathway Scaffold RASSF1A to Facilitate YAP/SMAD2 Nuclear Translocation. Mol Cell **2016**;63(1):156-66 doi 10.1016/j.molcel.2016.05.012.
17. Hannigan A, Smith P, Kalna G, Lo NC, Orange C, O'Brien DI*, et al.* Epigenetic downregulation of human disabled homolog 2 switches TGF-β from a tumor suppressor to a tumor promoter. J Clin Invest **2010**;120(8):2842-57.
18. Jiang P, Gu S, Pan D, Fu J, Sahu A, Hu X*, et al.* Signatures of T cell dysfunction and exclusion predict cancer immunotherapy response. Nat Med **2018**;24(10):1550-8 doi 10.1038/s41591-018-0136-1.
19. Ayers M, Lunceford J, Nebozhyn M, Murphy E, Loboda A, Kaufman DR*, et al.* IFN-gamma-related mRNA profile predicts clinical response to PD-1 blockade. J Clin Invest **2017**;127(8):2930-40 doi 10.1172/JCI91190.

SUPPLEMENTARY FIGURES (Yang et al)

Figure S1. Effect of TGF-β pathway antagonism on primary tumor and lung metastasis burden in all twelve breast cancer models

Figure S2. Effect of TGF-β pathway antagonism on lung metastasis is still evident if the start of treatment is delayed until after establishment of primary tumor

Figure S3. Representative capillary nanoimmunoassay (CNIA) dataset for assessment of Smad2 phosphorylation in 4T1 primary tumors following treatment with anti-TGF-β antibodies.

Figure S4. TGF-β isoform expression in primary tumors in the model panel.

Figure S5. TGF-β pathway signaling in the tumor models.

Figure S6. Brightfield proximity ligation assay for Smad complex formation in treatment-naïve primary tumors

Figure S7. TGF-β "switch" components in the different model classes.

Figure S8. Immunostaining for immune cell and other markers in untreated primary tumors from the 12 mouse metastatic breast cancer models.

Figure S9. *In vitro* responses to TGF-β of representative cell lines from InhibMet and StimMet models

Figure S10. Summary of candidate and discovery approaches to predictive biomarker identification.

Figure S11. Anti-TGF-β antibodies can still stimulate metastasis in the MVT1 StimMet model when combined with effective chemotherapy

Supplementary Figure S1 *(Yang et al.)*

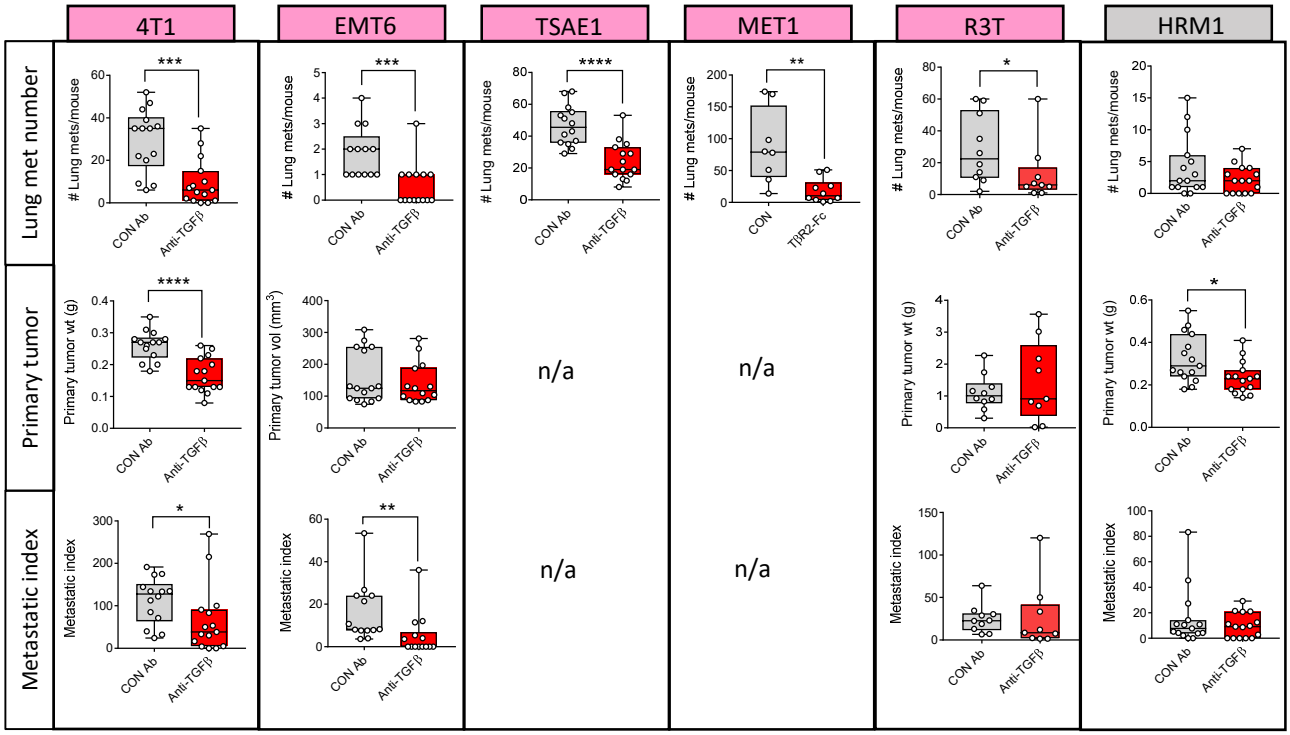

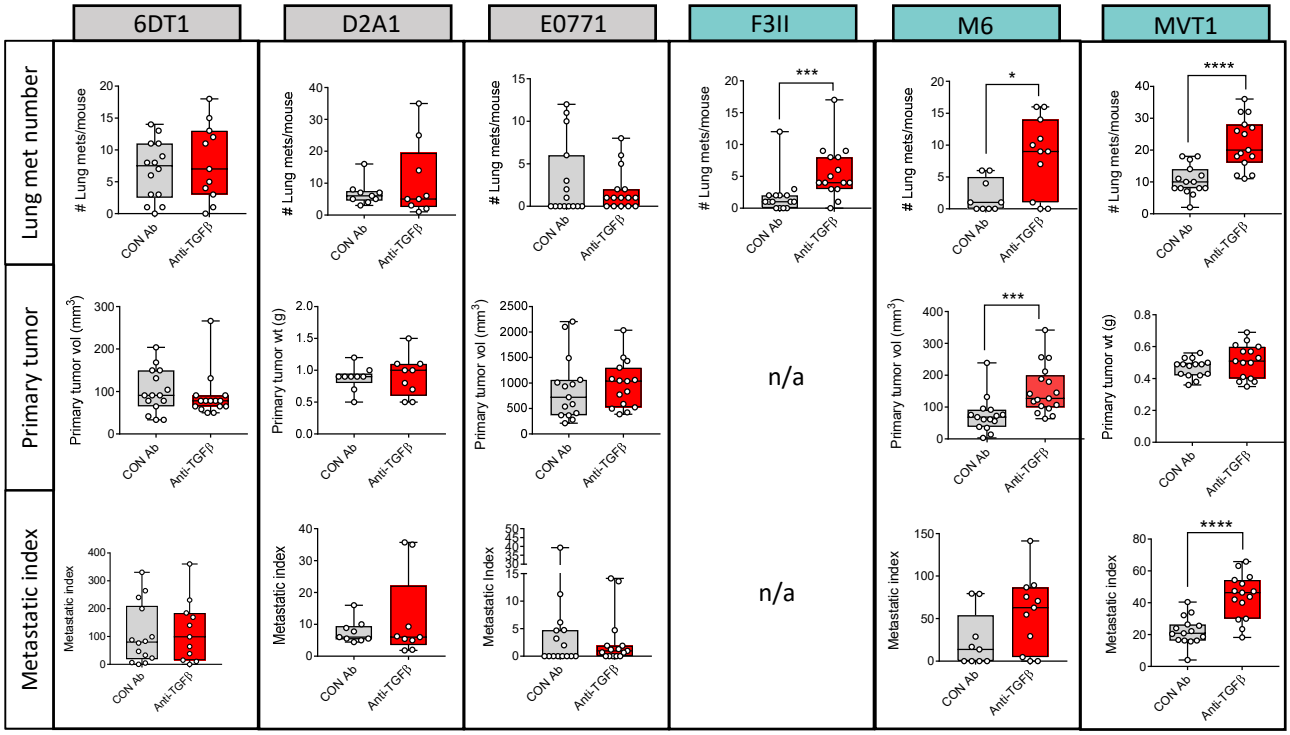

Legend on following page

Supplementary Figure S1 ***(Yang et al.)***

Figure S1. Effect of TGF-β pathway antagonism on primary tumor and lung metastasis burden in all twelve breast cancer models. Mice were treated with anti-TGF-β neutralizing antibody (1D11) or control antibody (13C4 or MOPC21), except for the MET1 model which was treated with a TGF-β ligand trap (TβR2Fc). For experimental details for each model, see Methods section. Results are median +/- IQ range (box) with whiskers indicating minimum and maximum values for n=10-15 mice/group. Statistics are Mann-Whitney test: *, $p<0.05$; **, $p<0.01$; ***$p<0.001$; ****$p<0.0001$. Models are grouped by response to therapy. Pink box indicates models for which metastasis is inhibited by anti-TGF-β antagonism (InhibMet models); grey box indicates no response to therapy (NoEff models); green box indicates stimulation of metastasis by TGF-β antagonism (StimMet models). For models that were run in the orthotopic implantation format, data are presented for number of lung metastases, size of primary tumor and number of lung metastases normalized to size of matched primary tumor ("metastatic index"). n/a, not applicable for models run in tail-vein injection format as no primary tumors formed.

Supplementary Figure S2 *(Yang et al.)*

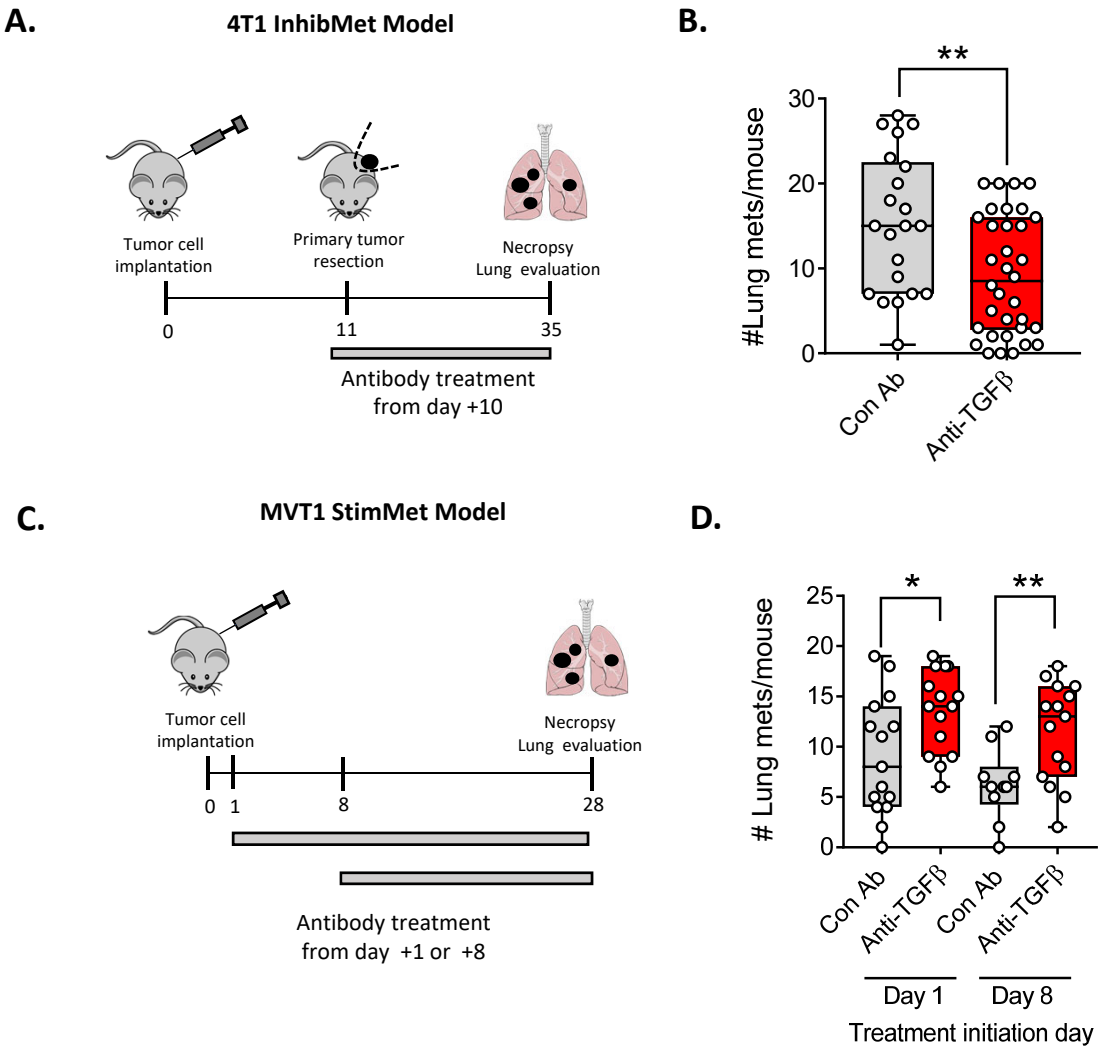

Figure S2. Effect of TGF-β pathway antagonism on lung metastasis is still evident if the start of treatment is delayed until after establishment of primary tumor. A,B. 4T1 InhibMet model. Mice were treated with anti-TGF-β neutralizing antibody (1D11) or control antibody (13C4), starting at day +10 after tumor cell implantation, when primary tumors are 0.8-1 cm diameter (schematic in A). Metastasis burden at endpoint was assessed histologically (B). Results are median +/- IQ range (box) with whiskers indicating minimum and maximum values for n=20 mice/group. Statistics are Mann-Whitney test: *, $p<0.05$; **, $p<0.01$. **C,D.** MVT1 StimMet model. Direct comparison of effect of antibody treatment starting at day +1 after tumor cell implantation or day +8 when primary tumors are well-established (>0.3cm diameter) (schematic in C). Metastasis burden at endpoint (D). Statistics as for B, but with n=8-15 mice/group.

Supplementary Figure S3 *(Yang et al.)*

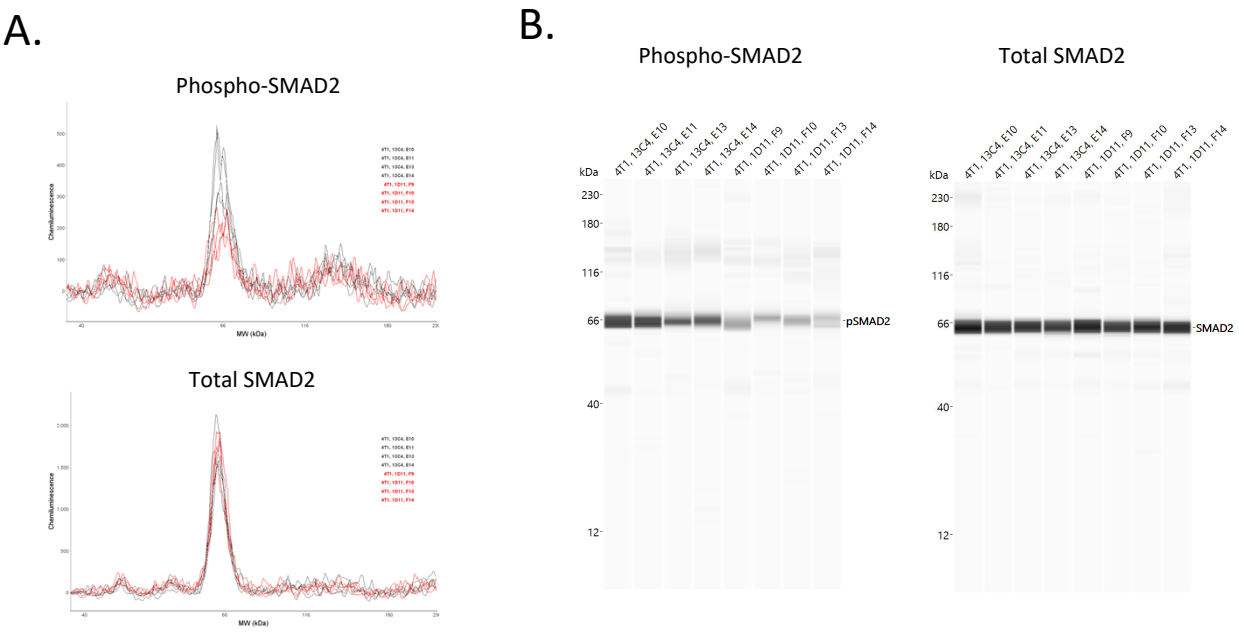

Figure S3. Representative capillary nanoimmunoassay (CNIA) dataset for assessment of SMAD2 phosphorylation in 4T1 primary tumors following treatment with anti-TGF-β antibodies. A. Chemiluminescence profiles from SimpleWestern nano-capillary immunoassay for phospho-Smad2 and total Smad2 levels in extracts from tumors treated with anti-TGF-β antibody (red) or isotype-matched control antibody (black). **B.** "Virtual Western" representation of the data in A. 4 independent tumors in each treatment group were assessed. Data was quantitated as area under the peak at ~66KDa in A.

Supplementary Figure S4 *(Yang et al.)*

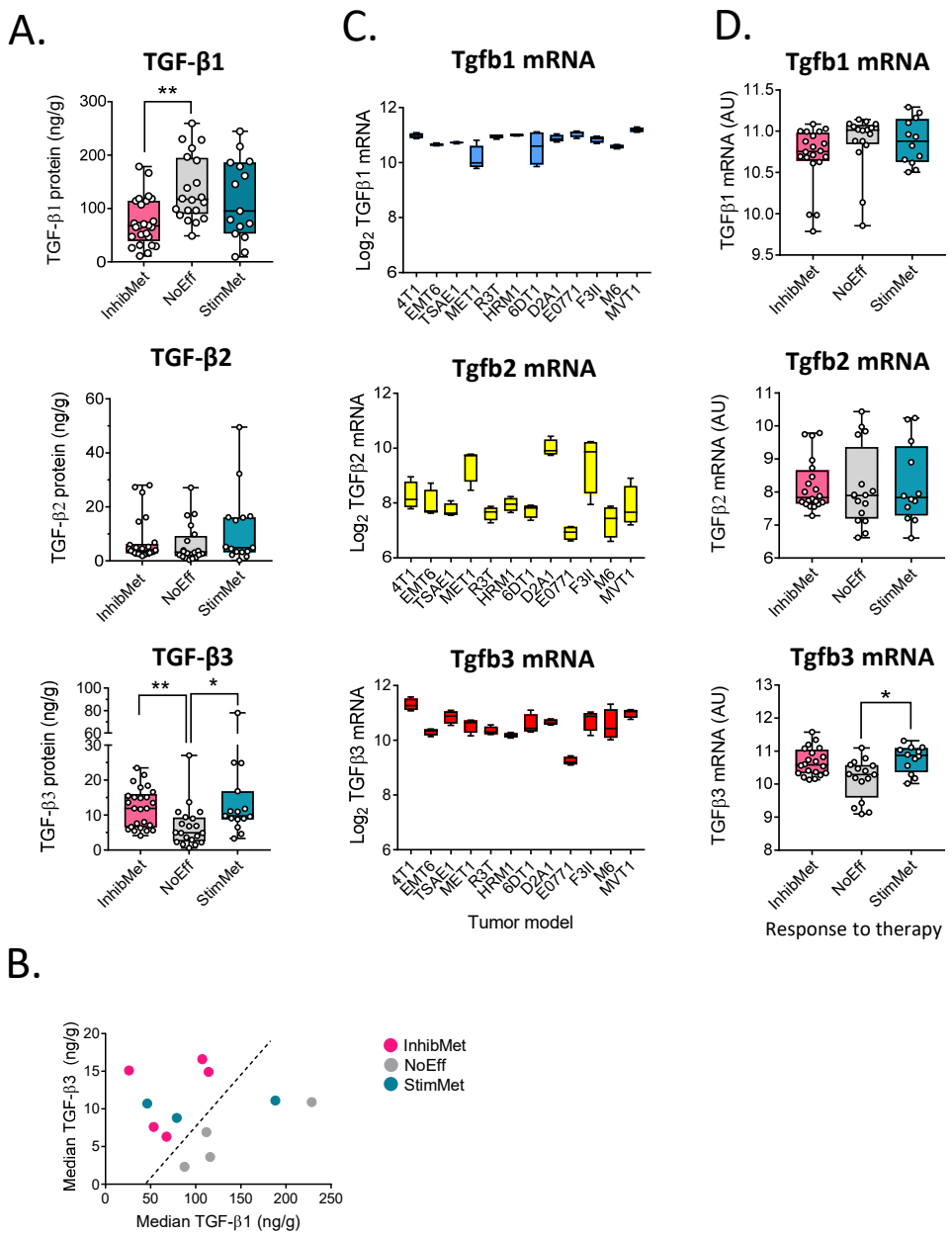

Figure S4. TGF-β isoform expression in primary tumors in the model panel. A. TGF-β1 and TGF-β3 isoform protein expression in acid-ethanol extracts of untreated primary tumors (median values for n=5/model). **B.** Median TGF-β1 and TGF-β3 protein levels for each model. Dotted line shows trend toward NoEff models having a combination of higher TGF-β1 and lower TGF-β3. **C,D.** TGF-β isoform mRNA expression in untreated primary tumors from each of the tumor models (n=4 tumors/model) from the microarray analysis. Results are median +/- IQ range (C). Results for all models are displayed grouped by therapeutic response class (D). Results are expressed as median +/- IQ range (box) with whiskers representing range. Statistics are Dunn's multiple comparison test. *, $p<0.05$; **, $p<0.01$

Supplementary Figure S5 *(Yang et al.)*

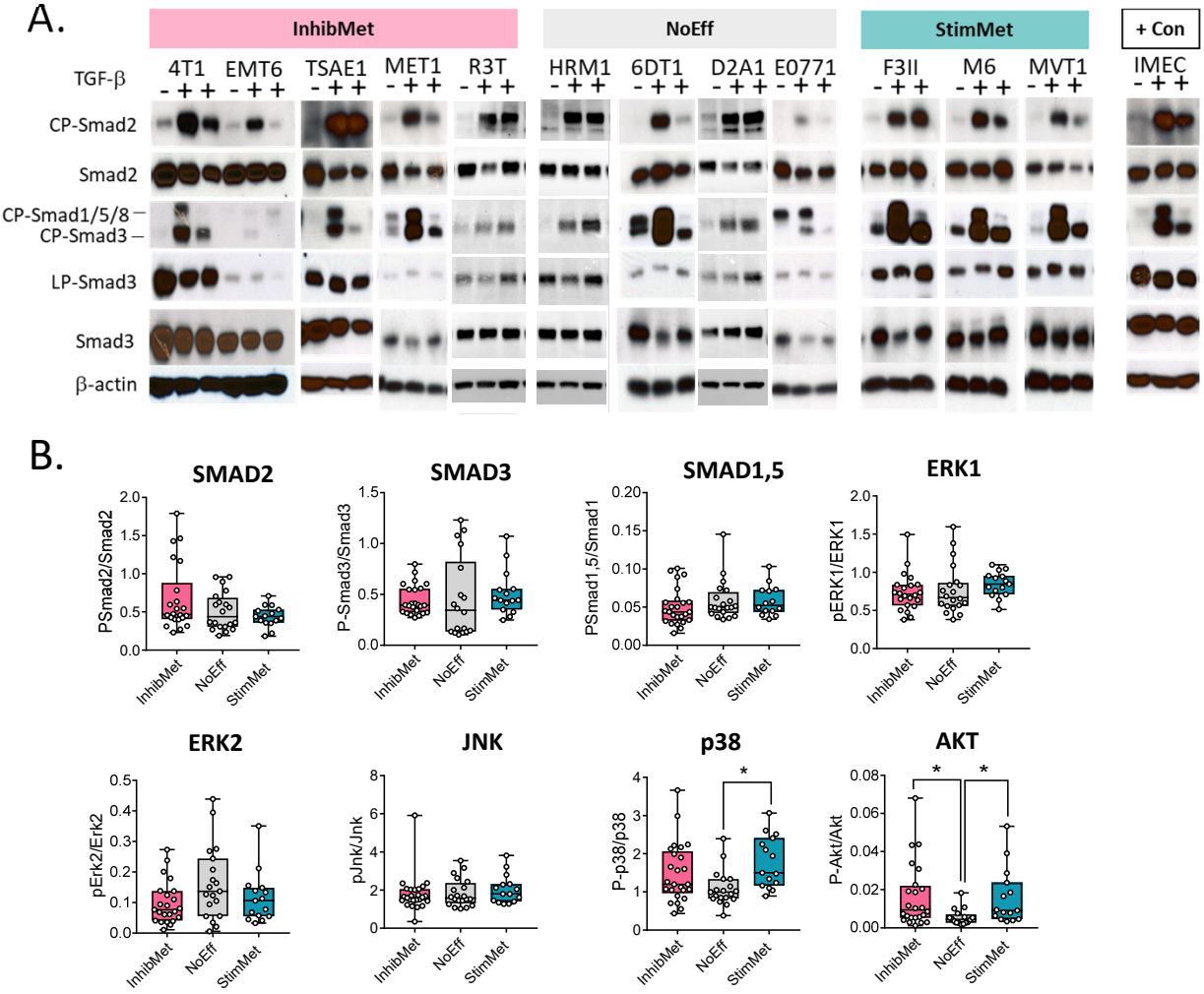

Figure S5. TGF-β pathway signaling in the tumor models. A. Conventional Western blot analysis of SMAD activation in cell lines from the twelve models following treatment with 5ng/ml TGF-β for 1 or 24 hours *in vitro*. CP, C-terminally phosphorylated SMAD; LP, linker phosphorylated SMAD. Cell lines are grouped by therapeutic response class. IMECs (conditionally immortalized mouse mammary epithelial cells) were included as a normal positive control. R3T, HRM1 and D2A1 were run in a later experiment and the batch of phospho-Smad3 antibody used was no longer detecting phospho-Smad1/5/8. **B.** Simple Western CNIA quantitation of activation of SMAD and non-SMAD signaling components downstream of TGF-β in untreated primary tumors for the different models. N=3-5 tumors/model; boxes show median +/- interquartile range with whiskers showing full range. Dunn's multiple comparisons test; *, $p<0.05$.

Supplementary Figure S6 *(Yang et al.)*

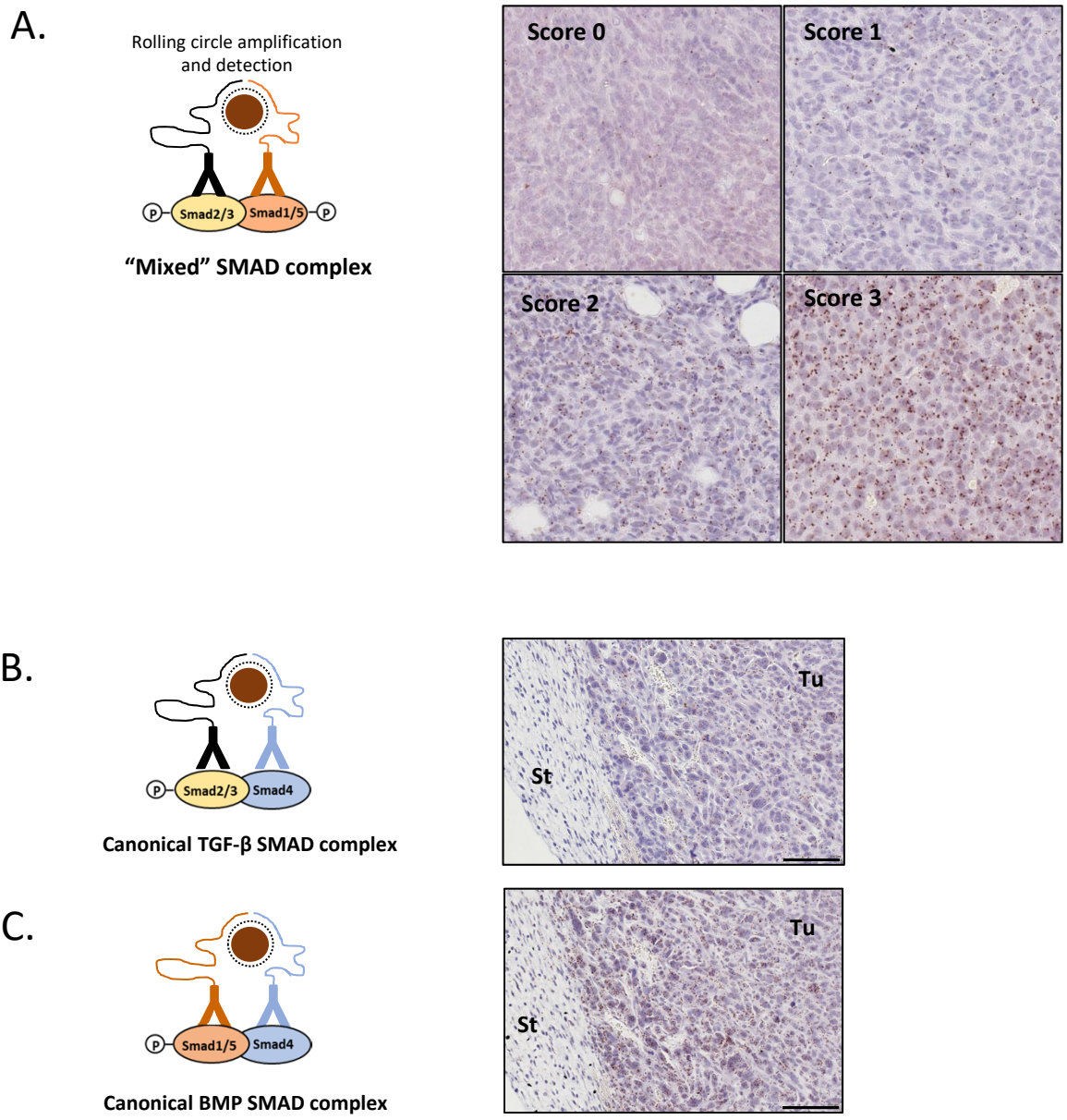

Figure S6. Brightfield proximity ligation assay for SMAD complex formation in treatment-naïve primary tumors. A. Schematic and representative images for brightfield PLA assay for mixed SMAD complex formation in untreated tumors showing examples in the four scoring categories. The PLA signal for complex formation appears as brown dots. **B,C.** Representative images for brightfield PLA assay for canonical TGF-β SMAD (**B**) and canonical BMP SMAD (**C**) complex formation in an untreated primary tumor from the TSAE1 model. In both cases the PLA signal is stronger in the tumor (Tu) than in the surrounding stroma (St). Scale bar represents 100µm.

Supplementary Figure S7 *(Yang et al.)*

A.

Gene or signature	P-value for association with Response Class (Kruskal-Wallis test)	Predicted status when TGF-β is tumor promoting (from literature)	Measured expression in InhibMet class
PSPC1	0.7319	Up	na
KLF5	0.5246	Up	na
YWHAZ (14-3-3z)	**0.0024**	**Up**	**Down**
SIX1	**0.0082**	**Up**	**Up**
PEAK1	0.1228	Up	na
RASSF1	0.1284	Down	na
DAB2	0.6533	Down	na
7-gene weighted	0.208	nd	na
7-gene unweighted	0.192	nd	na

B.

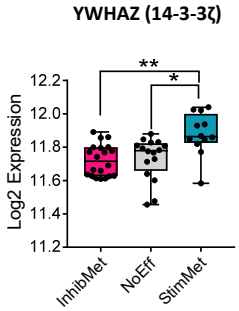

C.

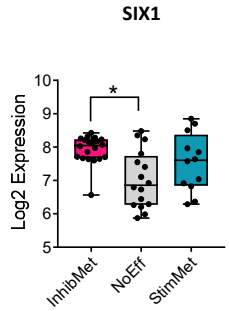

Figure S7. TGF-β "switch" components in the different model classes. A. Summary table showing TGF-β "switch components" and the p-values for association of their mRNA levels with therapeutic response class (Kruskal-Wallis test). Proposed TGF-β switch components were identified from the existing literature and their predicted relative expression in the InhibMet class (where TGF-β is tumor promoting and TGF-β antagonists are tumor suppressive) is compared with the experimentally measured expression in the InhibMet class relative to the other two classes (StimMet and NoEff). mRNA levels for the TGF-β "switch" components were assessed in the primary tumors of all twelve models (n=4/model) by microarray analysis. The 7-gene signature is the sum of expression of all 7 switch components. Expression values were either unweighted or weighted by the predicted direction of expression in the InhibMet class (+1 for up and -1 for down). Nd, not done; na, not applicable. **B,C.** Expression of YWHAZ (B) and SIX1 (C) in primary tumors from different response classes (median +/- IQ range, n=4 tumors/model, Dunn's multiple comparison test, *,$p<0.05$; **$p<0.01$). Note that association of Ywhaz with response class is opposite to that predicted from the literature.

Supplementary Figure S8 *(Yang et al.)*

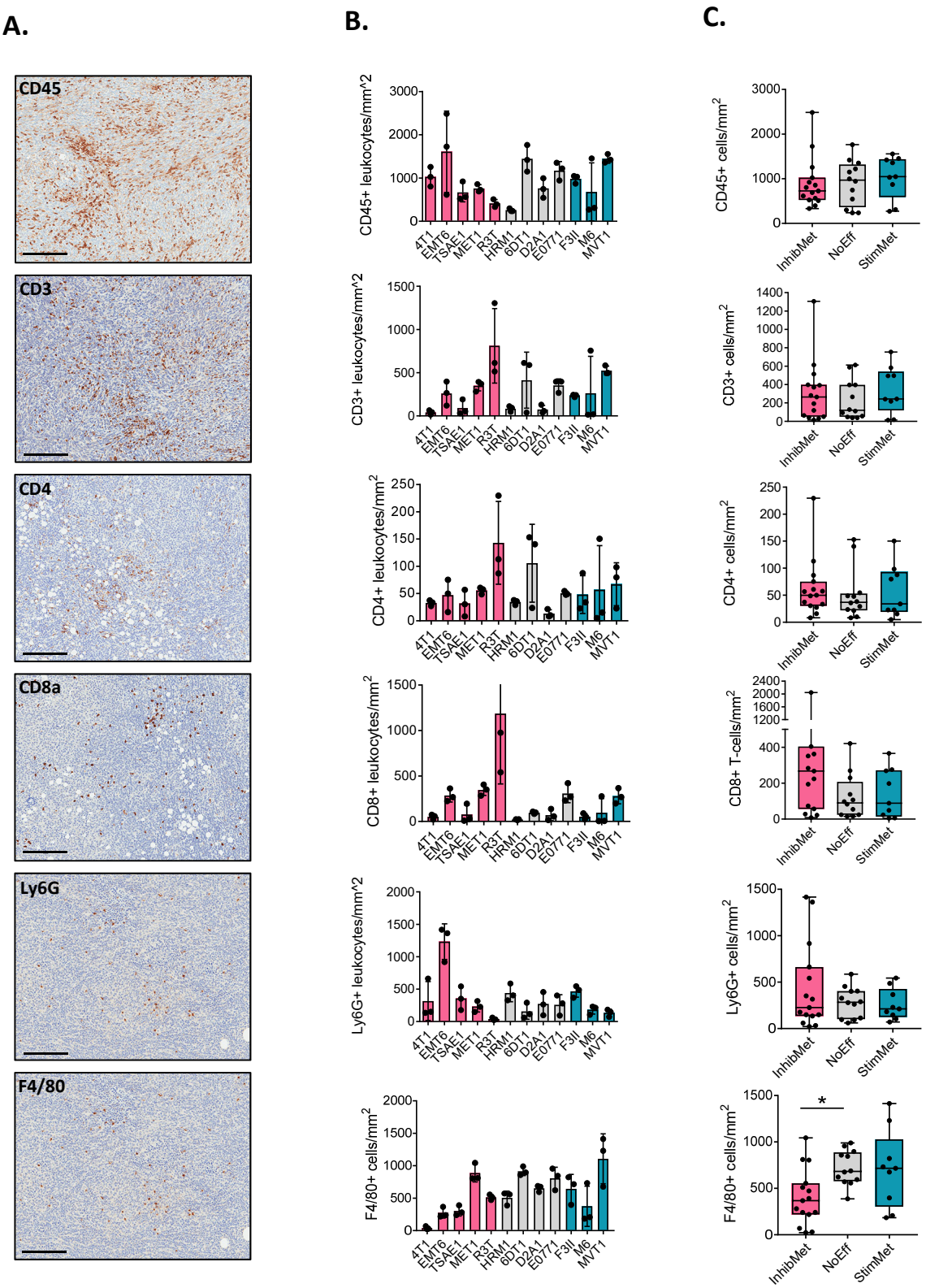

Supplementary Figure S8 cont. ***(Yang et al.)***

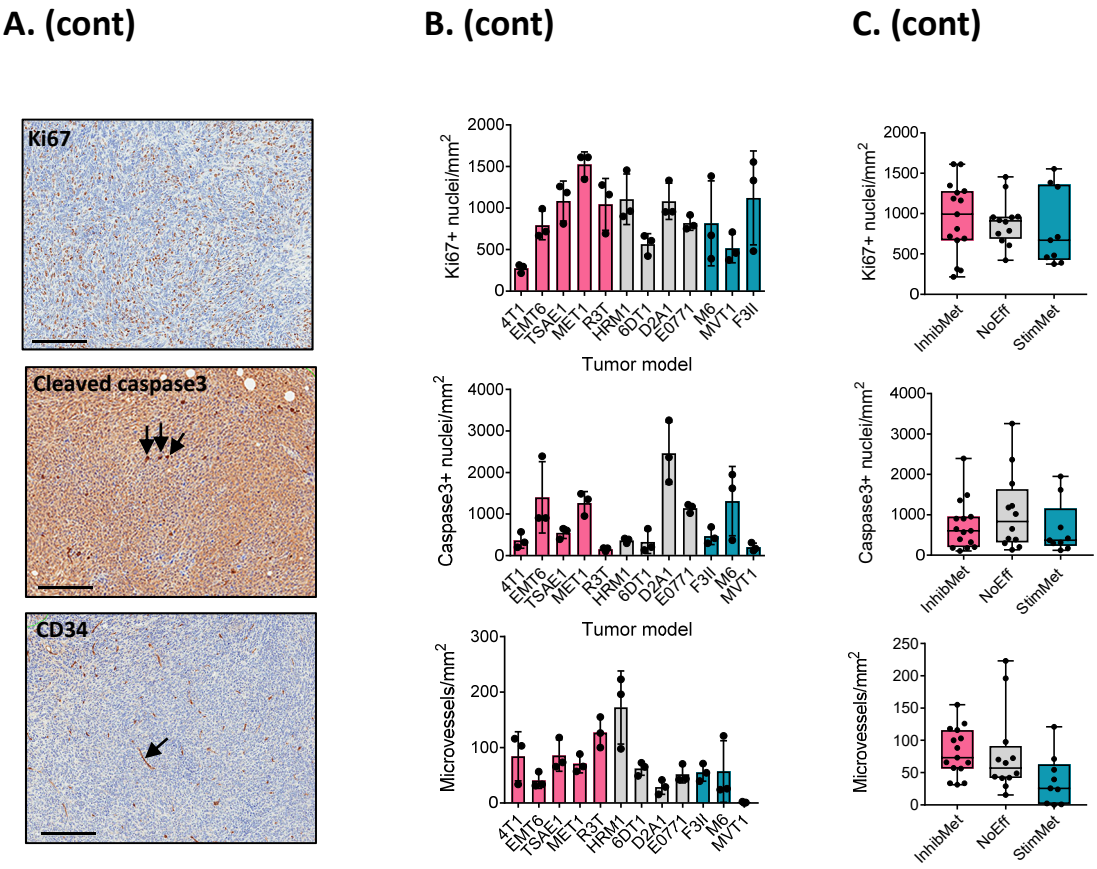

Figure S8. Immunostaining for immune cell and other markers in untreated primary tumors from the 12 mouse metastatic breast cancer models. A. Example images of immunostaining for individual markers. All images are from MVT1 tumors, except for F4/80 (HRM1), CD34 (6DT1) and cleaved Caspase 3 (EMT6). Scale bar is 200µm **B.** Semi-automated quantitation of # positive cells or structures (for microvessels)/mm^2 within the tumor. Results are mean +/- SD for n=3 tumors/model, shown for individual models. For details, see Supplementary Methods. **C.** Scores for individual tumors grouped by response class. Results are median +/- IQ range, Dunn's multiple comparison test. *, p<0.05.

Supplementary Figure S9 *(Yang et al.)*

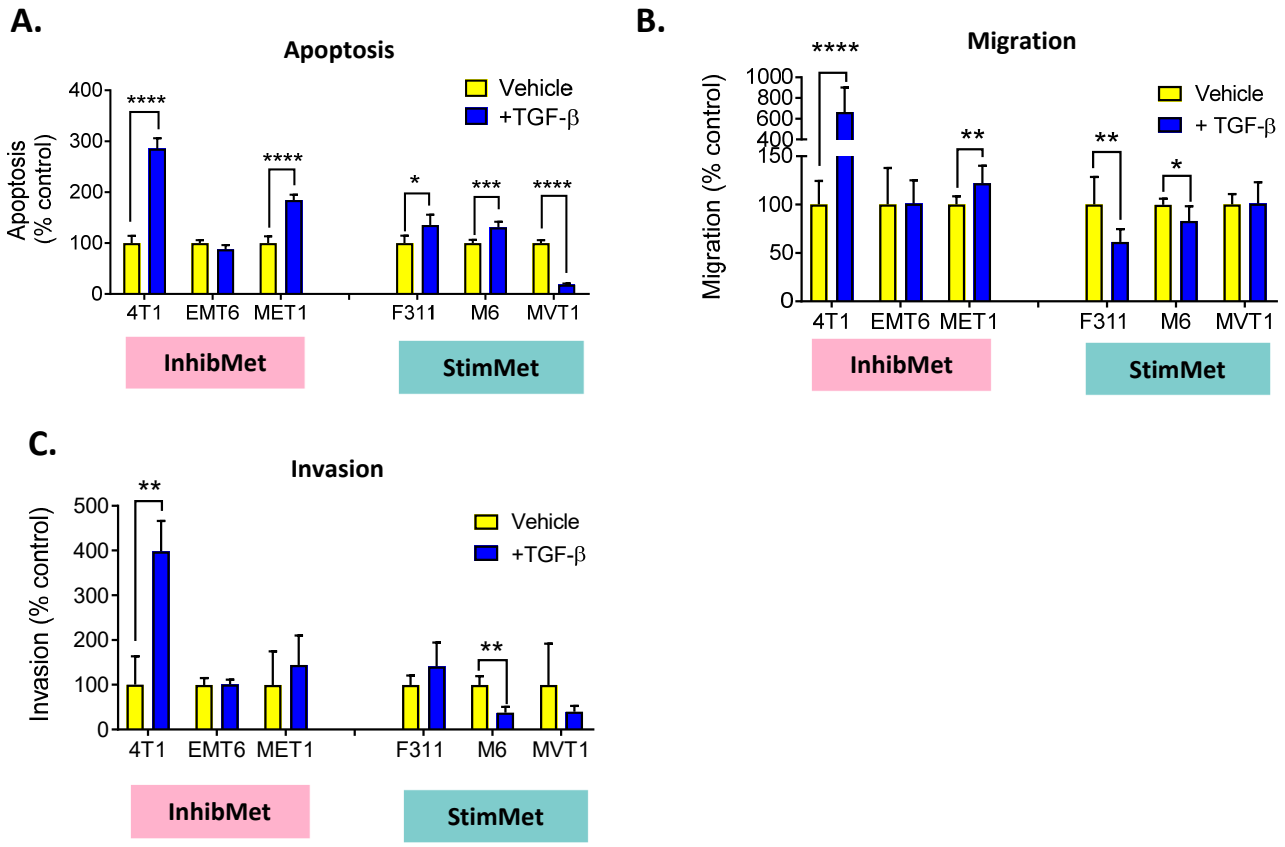

Figure S9. *In vitro* responses to TGF-β of representative cell lines from InhibMet and StimMet models. A. Apoptosis, B. Migration, and C. Invasion. All data are normalized to the vehicle control for the cell line and presented as mean +/- S.D., n=3, Student's t-test. *, p<0.05; **, p<0.01; ***, p<0.001; ****, p<0.0001

Supplementary Figure S10
(legend on next page)

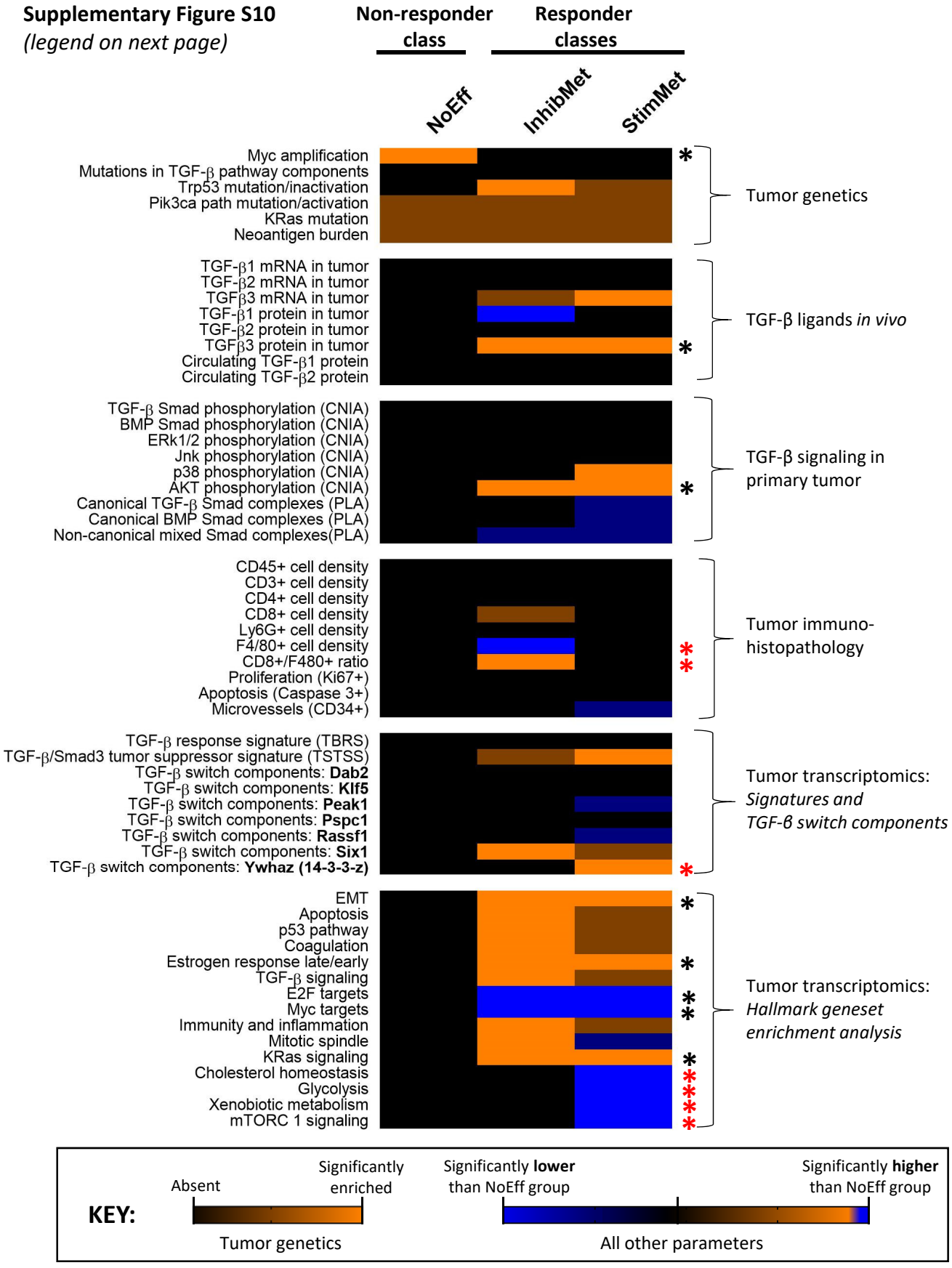

* May identify NoEff (non-responder group)

* May identify InhibMet from StimMet group

Supplementary Figure S10 (cont)

Figure S10. Summary of candidate and discovery approaches to predictive biomarker identification. The heatmap summarizes the relative representation (incidence compared to wildtype for tumor genetics; relative expression levels compared with the NoEff group for other markers) of the different biomarkers assessed in this study. In general, the two responder groups (InhibMet and StimMet) are more similar to each other than to the non-responder (NoEff) group. Black stars indicate markers that might be useful to distinguish the Responder (InhibMet and StimMet) from the non-responder (NoEff) groups. Red stars indicate markers that might be useful in distinguishing the InhibMet group from the StimMet group. However, most starred differences between the groups, while statistically significant at the cohort level, tend not to distinguish the response groups very robustly and may need to be used in combination with each other or additional markers. Further validation will be necessary. Geneset enrichment analyses highlighting biological differences in tumor transcriptomic datasets are the richest source of distinguishing features between the response classes, while individual marker analyses are generally less powerful.

Supplementary Figure S11 ***(Yang et al.)***

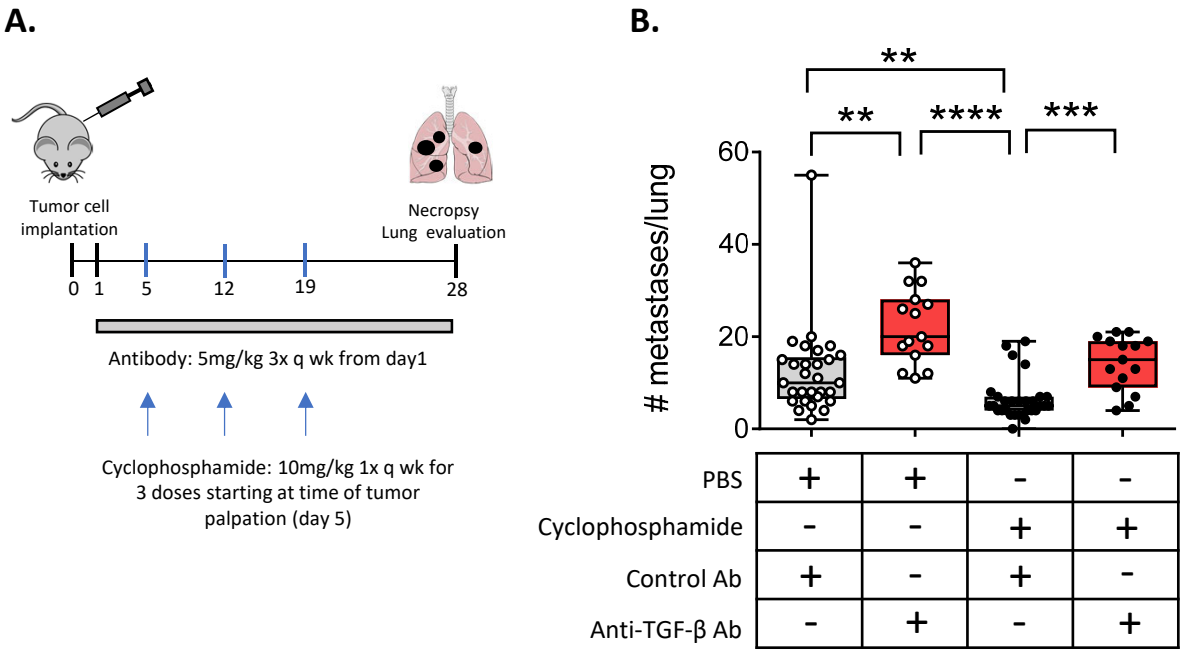

Figure S11. Anti-TGF-β antibodies can still stimulate metastasis in the MVT1 StimMet model when combined with effective chemotherapy A. Schematic for combination therapy with anti-TGF-β antibodies and cyclophosphamide in the MVT1 StimMet model. Drug and antibodies were delivered intraperitoneally. **B.** Lung metastatic burden in mice treated with anti-TGF-β and cyclophosphamide alone or in combination. Cyclophosphamide alone causes a statistically significant 2-fold decrease in metastatic burden, while anti-TGF-β causes a 2-fold increase that is still evident even in combination with cyclophosphamide. Boxes indicate median and interquartile ranges and whiskers indicate full range. Results are for n=15 mice/group (antibody-treated) or n=30 mice/group (control or cyclophosphamide alone). Statistics: Dunn's multiple comparison test, comparing all groups against each other. **, $p<0.01$; ***, $p<0.001$; ****, $p<0.0001$